Available online at www.sciencedirect.com
SCIENCE DIRECT®
Journal of Computational Physics 210 (2005) 386–399
JOURNAL OF COMPUTATIONAL PHYSICS
www.elsevier.com/locate/jcp

Two-dimensional time dependent Riemann solvers for neutron transport

Thomas A. Brunner [a,*], James Paul Holloway [b]

[a] Sandia National Laboratories,[1] HEDP Theory & ICF Target Design, P.O. Box 5800, Albuquerque, NM 87185-1186, United States
[b] Department of Nuclear Engineering and Radiological Sciences, University of Michigan, Ann Arbor, MI 48109-2014, United States

Received 15 December 2004; received in revised form 20 April 2005; accepted 25 April 2005
Available online 21 June 2005

Abstract

A two-dimensional Riemann solver is developed for the spherical harmonics approximation to the time dependent neutron transport equation. The eigenstructure of the resulting equations is explored, giving insight into both the spherical harmonics approximation and the Riemann solver. The classic Roe-type Riemann solver used here was developed for one-dimensional problems, but can be used in multidimensional problems by treating each face of a two-dimensional computation cell in a locally one-dimensional way. Several test problems are used to explore the capabilities of both the Riemann solver and the spherical harmonics approximation. The numerical solution for a simple line source problem is compared to the analytic solution to both the P_1 equation and the full transport solution. A lattice problem is used to test the method on a more challenging problem.

Keywords: Riemann solvers; Time dependent transport; Spherical harmonics; Finite methods; Radiative transfer

1. Introduction

Riemann solvers are a class of numerical methods for solving time dependent hyperbolic systems of equations. These extremely robust solvers were originally developed for fluid dynamics problems where shocks may arise. Since then, they have been used on many different problems, including traffic flow,

* Corresponding author. Tel.: +1 505 844 1253; fax: +1 505 845 7820.
E-mail address: tabrunn@sandia.gov (T.A. Brunner).
[1] Sandia is a multiprogram laboratory operated by Sandia Corporation, a Lockheed Martin Company, for the United States Department of Energy and National Nuclear Security Administration under Contract DE-AC04-94AL85000.

0021-9991/$ - see front matter © 2005 Elsevier Inc. All rights reserved.
doi:10.1016/j.jcp.2005.04.011

plasma simulations [1], and two-phase flow calculations for nuclear reactor systems [2]. Recently, Riemann solvers have been applied to radiation hydrodynamics [3–5]. These calculations model the radiation transport using a synthetic diffusion description with Eddington factors fixed from an external transport calculation.

We have previously described in detail how to apply Riemann solvers to the spherical harmonics expansion of the transport equation in one dimension [6,7]. Here we will present a brief summary of the one-dimensional problem, then extend it to two dimensions. As will be described below, multidimensional problems can be treated by using the one-dimensional numerical flux across each of the faces in a multi-dimensional computation cell.

2. Spherical harmonics

One common approximation used to solve the transport equation is based on expanding the angular flux $\psi(\mathbf{\Omega})$ in terms of the spherical harmonics $Y_l^m(\mathbf{\Omega})$. This is most frequently done in one dimension; here we will do a full three-dimensional expansion and then simplify to fewer dimensions. Since we are mainly concerned with the treatment of the streaming operator, only absorption and isotropic scattering are considered here. It is easy to add higher scattering moments [8,9] or more complicated scattering processes.

2.1. The expansion

The spherical harmonic functions are defined as [10]

$$Y_l^m(\mu,\varphi) = (-1)^m \sqrt{\frac{2l+1}{4\pi}\frac{(l-m)!}{(l+m)!}}\frac{(1-\mu^2)^{m/2}}{2^l l!}\mathrm{e}^{\mathrm{i}m\varphi}\frac{\mathrm{d}^{l+m}}{\mathrm{d}\mu^{l+m}}(\mu^2-1)^l, \tag{1}$$

where $l \geqslant 0$ and $0 \leqslant m \leqslant l$. There is a slightly modified form for $m < 0$, but these terms are not needed here because the angular flux is real. The spherical harmonics form a complete set of orthonormal basis functions, and we can expand the angular flux as

$$\psi(\mathbf{x},\mathbf{\Omega}) = \sum_{l=0}^{\infty}\sum_{m=-l}^{l}\psi_l^m(\mathbf{x})Y_l^m(\mathbf{\Omega}), \quad \text{where } \psi_l^m(\mathbf{x}) = \int_{4\pi}\overline{Y}_l^m\psi(\mathbf{x},\mathbf{\Omega})\,\mathrm{d}\mathbf{\Omega}. \tag{2}$$

This expansion is exact, but in order to make practical use of it, the series must be truncated. The P_N approximation is based on the assumption that all $\psi_l^m = 0$ for $l > N$.

Various spherical harmonic moments of ψ can be interpreted as physical quantities. The ψ_0^0 moment is simply the density of particles multiplied by their speed v, the well-known scalar flux. The ψ_1^m terms are related to the momentum of the particles, the neutron current, and the ψ_2^m terms are related to pressure.

Expanding the three-dimensional Boltzmann transport equation yields

$$\begin{aligned}&\frac{\partial}{\partial t}\psi_l^m + \frac{1}{2}\frac{\partial}{\partial x}\left(-C_{l-1}^{m-1}\psi_{l-1}^{m-1} + D_{l+1}^{m-1}\psi_{l+1}^{m-1} + E_{l-1}^{m+1}\psi_{l-1}^{m+1} - F_{l+1}^{m+1}\psi_{l+1}^{m+1}\right)\\ &\quad + \frac{1}{2}\mathrm{i}\frac{\partial}{\partial y}\left(C_{l-1}^{m-1}\psi_{l-1}^{m-1} - D_{l+1}^{m-1}\psi_{l+1}^{m-1} + E_{l-1}^{m+1}\psi_{l-1}^{m+1} - F_{l+1}^{m+1}\psi_{l+1}^{m+1}\right) + \frac{\partial}{\partial z}\left(A_{l-1}^m\psi_{l-1}^m + B_{l+1}^m\psi_{l+1}^m\right)\\ &\quad + \Sigma_t\psi_l^m = \Sigma_s\psi_0^0\delta_{l0}\delta_{m0}\end{aligned} \tag{3}$$

for $0 \leqslant l < \infty$ and $-l \leqslant m \leqslant l$, with

$$A_l^m = \sqrt{\frac{(l-m+1)(l+m+1)}{(2l+3)(2l+1)}}, \quad B_l^m = \sqrt{\frac{(l-m)(l+m)}{(2l+1)(2l-1)}}, \tag{4}$$

$$C_l^m = \sqrt{\frac{(l+m+1)(l+m+2)}{(2l+3)(2l+1)}}, \quad D_l^m = \sqrt{\frac{(l-m)(l-m-1)}{(2l+1)(2l-1)}}, \tag{5}$$

$$E_l^m = \sqrt{\frac{(l-m+1)(l-m+2)}{(2l+3)(2l+1)}}, \quad F_l^m = \sqrt{\frac{(l+m)(l+m-1)}{(2l+1)(2l-1)}}. \tag{6}$$

Because ψ is real, we can use a property of spherical harmonics, namely

$$\overline{Y}_l^m = (-1)^m Y_l^{-m} \Rightarrow \overline{\psi}_l^m(\mathbf{x}) = (-1)^m \psi_l^{-m}, \tag{7}$$

to reduce the number of unknowns. With this we can eliminate all terms with $m < 0$ simply by using the complex conjugate of the appropriate moment with a positive m.

Many problems are two-dimensional in nature and do not need the full treatment Eq. (3) can give. In a two-dimensional system there is no change in any of the variables along a particular direction. Inspecting Eq. (3) suggests the y dependence be dropped. This choice decouples the real and imaginary parts of the equations, and we only need to solve for the real parts. This leaves us with

$$\begin{aligned}&\frac{\partial}{\partial t}\psi_l^m + \frac{1}{2}\frac{\partial}{\partial x}\left(-C_{l-1}^{m-1}\psi_{l-1}^{m-1} + D_{l+1}^{m-1}\psi_{l+1}^{m-1} + E_{l-1}^{m+1}\psi_{l-1}^{m+1} - F_{l+1}^{m+1}\psi_{l+1}^{m+1}\right)\\ &\quad + \frac{\partial}{\partial z}\left(A_{l-1}^m\psi_{l-1}^m + B_{l+1}^m\psi_{l+1}^m\right) + \Sigma_t\psi_l^m = 0\end{aligned} \tag{8}$$

for $m \neq 0$ and for $m = 0$ we have

$$\frac{\partial}{\partial t}\psi_l^0 + \frac{\partial}{\partial x}\left(E_{l-1}^1\psi_{l-1}^1 - F_{l+1}^1\psi_{l+1}^1\right) + \frac{\partial}{\partial z}\left(A_{l-1}^0\psi_{l-1}^0 + B_{l+1}^0\psi_{l+1}^0\right) + \Sigma_t\psi_l^0 = \Sigma_s\psi_0^0\delta_{l0}, \tag{9}$$

where we have used $C_l^{-1} = E_l^1$ and $D_l^{-1} = F_l^1$ to eliminate the $m = -1$ terms from the $m = 0$ case.

2.2. The eigenstructure

In order to use the P_N approximation with a Riemann solver, we need to determine the eigenstructure of the system. One of the more commonly used Riemann solvers is a Roe-type Riemann solver. In a Roe-type solver, a nonlinear system is linearized in a specific manner. Because the spherical harmonics system is linear, all of the properties of the linearized Roe matrix are automatically met by the Jacobian. The eigenstructure of the z Jacobian is particularly easy to determine analytically and will be shown here.

Inspecting Eq. (3), we see that each of the azimuthal (m) modes is decoupled from the other azimuthal modes. If we group the equations by identical values of m, the Jacobian is a block diagonal matrix. The eigenstructure of each block is independent of the others. One block of the z Jacobian looks like

$$\mathbf{A}_z^m = \begin{bmatrix} 0 & B_{m+1}^m & 0 & \cdots & & & \\ & & \cdots & & & & \\ \cdots & 0 & A_{l-1}^m & 0 & B_{l+1}^m & 0 & \cdots \\ & & & & \cdots & & \\ & & & \cdots & 0 & A_{N-1}^m & 0 \end{bmatrix}, \tag{10}$$

where each block contains the $m + 1 \leqslant l \leqslant N - 1$ modes. If we multiply a vector of Y_l^m's by the Jacobian, there results

$$\begin{bmatrix} 0 & B^m_{m+1} & 0 & \dots & & & \\ & & \dots & & & & \\ \dots & 0 & A^m_{l-1} & 0 & B^m_{l+1} & 0 & \dots \\ & & & \dots & & & \\ & & & \dots & 0 & A^m_{N-1} & 0 \end{bmatrix} \begin{bmatrix} Y^m_m \\ \dots \\ Y^m_l \\ \dots \\ Y^m_N \end{bmatrix} = \begin{bmatrix} B^m_{m+1} Y^m_{m+1} \\ \dots \\ A^m_{l-1} Y^m_{l-1} + B^m_{l+1} Y^m_{l+1} \\ \dots \\ A^m_{N-1} Y^m_{N-1} \end{bmatrix}. \tag{11}$$

But this is practically the recursion relation $Y^m_l \cos\theta = A^m_l Y^m_{l+1} + B^m_l Y^m_{l-1}$, namely

$$\begin{bmatrix} B^m_{m+1} Y^m_{m+1} \\ \dots \\ A^m_{l-1} Y^m_{l-1} + B^m_{l+1} Y^m_{l+1} \\ \dots \\ A^m_{N-1} Y^m_{N-1} \end{bmatrix} = \begin{bmatrix} A^m_m Y^m_{m+1} \\ \dots \\ B^m_l Y^m_{l-1} + A^m_l Y^m_{l+1} \\ \dots \\ B^m_N Y^m_{N-1} \end{bmatrix} = \mu \begin{bmatrix} Y^m_m \\ \dots \\ Y^m_l \\ \dots \\ Y^m_N \end{bmatrix}, \tag{12}$$

where $\mu = \cos\theta$. For the last line to work as the recursion relation, we need

$$Y^m_{N+1}(\mu, \varphi) = 0. \tag{13}$$

The eigenvalues are just μ's from the solution of Eq. (13) for each $0 \leqslant m \leqslant N$. The right eigenvectors for each of the m blocks are the spherical harmonics evaluated at these μ_k's. The eigenvectors for the entire Jacobian are just these eigenvectors for the m blocks padded with zeros. (The P_1 eigenvectors are shown in Eq. (16).) The value of φ is immaterial; for fixed m as φ varies the eigenvector is just multiplied by the scalar $e^{im\varphi}$. Because $A^m_{l-1} = B^l_m$, the Jacobian is symmetric, and the left eigenvectors are the same as the right eigenvectors, and each is normalized such that $\mathbf{r}_k \cdot \mathbf{r}_k = 1$. The special case of the A^0_z block of the Jacobian is the matrix describing the one-dimensional Legendre polynomial expansion of the transport equation [6,11].

The eigenvalues are all real and in the range $-1 < \mu < 1$. Each eigenvalue is unique with one exception; there can be multiple zero eigenvalues. For all odd N, these zeros only occur in the blocks with $m > 0$.

Some insight may be gained by looking at a specific example. The Jacobian in front of the z derivative for the two-dimensional P_1 approximation is

$$\mathbf{A}_z = \begin{bmatrix} 0 & \sqrt{\frac{1}{3}} & 0 \\ \sqrt{\frac{1}{3}} & 0 & 0 \\ 0 & 0 & 0 \end{bmatrix}. \tag{14}$$

As mentioned above, $\mathbf{A}_z$ is symmetric. This means if we normalize each of the k right eigenvectors such that

$$\mathbf{r}_k \cdot \mathbf{r}_k = 1, \tag{15}$$

they are also the left eigenvectors, so we have

$$\mathbf{r} = \mathbf{l} = \left\{ \begin{bmatrix} \frac{1}{\sqrt{2}} \\ -\frac{1}{\sqrt{2}} \\ 0 \end{bmatrix}, \begin{bmatrix} 0 \\ 0 \\ 1 \end{bmatrix}, \begin{bmatrix} \frac{1}{\sqrt{2}} \\ \frac{1}{\sqrt{2}} \\ 0 \end{bmatrix} \right\}. \tag{16}$$

The corresponding eigenvalues of this matrix are

$$\lambda = \left\{ -\frac{1}{\sqrt{3}}, 0, \frac{1}{\sqrt{3}} \right\}. \tag{17}$$

The first and last eigenvectors represent particles (scalar flux) and momentum (current) traveling in the z direction with speed $\pm 1/\sqrt{3}$. The middle eigenvector is simply a statement that the x current is not transported in the z direction.

For even N, there is also zero eigenvalue in the $m = 0$ block of the Jacobian. This eigenvector contains particles (there is a Y_0^0 component), but because the wave speed associated with this wave is zero, these particles do not move. It is this fact that causes the P_N approximations with even N to give unusual results; the even N approximations have historically been avoided because of this [9].

The eigensystems vary in size depending on the order of the P_N approximation. In two dimensions, the number of spherical harmonic moments is $(N^2 + 3N)/2 + 1$, so for P_1, P_9, and P_{15} there are 3, 55, and 136 moments, respectively. Because of the large size of the systems, *MATLAB* is used in practice to construct each of the Jacobians, and the eigenstructure is determined numerically once before the simulation begins.

3. The Riemann solver

After averaging over a spatial cell, our system of equations, Eqs. (8) and (9), can be written in vector form as

$$\frac{\partial \mathbf{u}_{i,j}}{\partial t} + \frac{\mathbf{A}_x \mathbf{u}_{i+1/2,j} - \mathbf{A}_x \mathbf{u}_{i-1/2,j}}{\Delta x} + \frac{\mathbf{A}_z \mathbf{u}_{i,j+1/2} - \mathbf{A}_z \mathbf{u}_{i,j-1/2}}{\Delta z} = \mathbf{S}_{i,j}, \tag{18}$$

where $\mathbf{u}_{i,j}$ is a vector of the cell averages of the ψ_l^m moments in the cell centered at (x_i, z_j) at time t, $\mathbf{S}_{i,j}$ contains the scattering terms, $\mathbf{A}_x u_{i\pm 1/2,j}$ is the flux of each the moments in the x direction, and similarly for the z direction. (The Riemann solver community simply calls $\mathbf{Au}$ the flux; we already have the angular flux and the scalar flux, and will understand "flux" without an adjective to mean this rate of flow of a state $\mathbf{u}$ across an interface.) The fluxes at the cell interfaces, $\mathbf{A}_x u_{i\pm 1/2,j}$ and $\mathbf{A}_z \mathbf{u}_{i,j\pm 1/2}$, must be computed somehow.

The Roe-type Riemann solver provides a very nice scheme for calculating solutions to time dependent problems in one dimension. But once a one-dimensional Riemann solver is constructed for a particular system of equations, it is easy to extend it to multiple dimensions. The simplest multidimensional Riemann solvers treat each of the directions individually, as if it were a set of one-dimensional problems [12]. This method is the one used here for the two-dimensional calculations and can be extended to three-dimensional calculations as well.

3.1. A one-dimensional Riemann solver

Consider a generic system of linear conservation equations describing a physical system,

$$\frac{\partial \mathbf{u}}{\partial t} + \frac{\partial \mathbf{A}\mathbf{u}}{\partial x} = \mathbf{S}(\mathbf{u}), \tag{19}$$

where $\mathbf{u}(x,t)$ is a vector of state variables, such as the spherical harmonic moments ψ_l^m, $\mathbf{Au}$ is called the flux of $\mathbf{u}$, and describes how the state variables change with variations in space, $\mathbf{S}(\mathbf{u})$ is a source vector, with terms that may or may not depend on $\mathbf{u}$, and $\mathbf{A}$ contains the coefficients from one of the terms in Eq. (3) or Eqs. (8) and (9). The source terms can include local terms such as collisions, body forces and external sources.

Riemann solvers give us a way to compute the solution of equations similar to Eq. (19). The numerical approximation to Eq. (19) begins by dividing space into cells with edges at $x_{i+1/2}$ and uniform widths Δx, although this restriction can be relaxed. Integrating $\mathbf{u}(x,t)$ over a spatial cell and dividing by Δx, we get space-averaged data in cell i at time t,

$$\mathbf{u}_i(t) = \frac{1}{\Delta x}\int_{x_{i-1/2}}^{x_{i+1/2}} \mathbf{u}(x,t)\,\mathrm{d}x. \tag{20}$$

Integrating Eq. (19) over space cell i yields

$$\frac{\partial \mathbf{u}_i}{\partial t} + \frac{\mathbf{A}\mathbf{u}_{i+1/2} - \mathbf{A}\mathbf{u}_{i-1/2}}{\Delta x} = \mathbf{S}_i, \tag{21}$$

where $\mathbf{u}_{i\pm1/2} = \mathbf{u}(x_{i\pm1/2}, t)$. Riemann solvers give us a means to determine the fluxes $\mathbf{A}\mathbf{u}_{i\pm1/2}$ at both the interior cell edges and the system boundaries. This clearly gives us a conservative numerical method.

3.1.1. A simplified problem to find the numerical fluxes

We need a way to approximate $\mathbf{A}\mathbf{u}_{i\pm1/2}$ between cell i and $i \pm 1$. Riemann solvers use the solution, $\tilde{\mathbf{u}}$, to a simplified hyperbolic problem to estimate the flux $A\mathbf{u}_{i\pm1/2}$ at the cell boundaries. The solution of a hyperbolic problem with piecewise constant initial data is known as the Riemann problem; it is from this that Riemann solvers take their name. This approximate solution is computed using the nearby cell averages of $\mathbf{u}$.

Consider the generic situation of an interface at $x = 0$, with discontinuous initial data $\mathbf{u}_r$ and $\mathbf{u}_\ell$ to the right and left of this interface, and consider $\tilde{\mathbf{u}}$ satisfying

$$\frac{\partial \tilde{\mathbf{u}}}{\partial t} + \mathbf{A}\frac{\partial \tilde{\mathbf{u}}}{\partial x} = 0 \tag{22}$$

with the initial condition

$$\tilde{\mathbf{u}}(x,0) = \begin{cases} \mathbf{u}_\ell & \text{if } x < 0, \\ \mathbf{u}_r & \text{if } x > 0. \end{cases} \tag{23}$$

Solving this system of equations [12–14,6,11,7,1], we get $\mathbf{A}\tilde{\mathbf{u}}(0,t)$ as

$$\mathbf{A}\tilde{\mathbf{u}}(0,t) = \sum_{\lambda_k>0} \lambda_k(\mathbf{l}_k\cdot\mathbf{u}_\ell)\mathbf{r}_k + \sum_{\lambda_k<0} \lambda_k(\mathbf{l}_k\cdot\mathbf{u}_r)\mathbf{r}_k. \tag{24}$$

Eq. (24) shows why Riemann solvers are so robust; they only use upwind information. We can also rewrite Eq. (24), in the form commonly used by the Riemann solver community, as

$$\mathbf{A}\tilde{\mathbf{u}}(0,t) = \frac{1}{2}(\mathbf{A}\mathbf{u}_\ell + \mathbf{A}\mathbf{u}_r) - \frac{1}{2}\sum_k \mathbf{r}_k|\lambda_k|(\mathbf{l}_k\cdot\Delta\mathbf{u}), \tag{25}$$

where $\Delta\mathbf{u} = \mathbf{u}_r - \mathbf{u}_\ell$. If we now, at each interface $i \pm 1/2$, somehow relate $\mathbf{u}_\ell$ and u_r to the cell states u_j for j near i, we can approximate Eq. (21) by using $\mathbf{A}\tilde{\mathbf{u}}$ to estimate $\mathbf{A}\mathbf{u}_{i\pm1/2}$, resulting in a spatially discretized system of equations. For example, the most natural choice at interface $i + 1/2$ would be $\mathbf{u}_\ell = \mathbf{u}_i$ and $u_r = \mathbf{u}_{i+1}$; Eq. (25) can then be seen as a centered difference with some dissipation added to make the scheme upwinded.

3.1.2. A high-resolution scheme

The flux based on $\mathbf{u}_\ell = \mathbf{u}_i$ and $\mathbf{u}_r = \mathbf{u}_{i+1}$ would lead to a method that is only first-order in space. It is possible to modify this Roe-type Riemann solver to be higher order in space [12], making it a high-resolution scheme. The basic premise is to compute $\mathbf{u}_\ell$ and $\mathbf{u}_r$ at each interface by using linear interpolation within the cell, respectively, to the left, and to the right, of the interface. In doing so, a slope must be computed for each state variable in each cell, using only nearby cell values; if this slope is computed as only a linear function of the cell state values the method can still only be first-order if artificial oscillations are prevented [1]. Therefore, we must use some nonlinear method to calculate the slope, and we must also do this carefully so that no new local minima or maxima are created.

One slope reconstruction method was first proposed by van Leer [14]. On a uniform mesh, each of the slopes are first calculated to the left and the right of cell i,

$$m_- = \frac{u_i - u_{i-1}}{\Delta x}, \tag{26}$$

$$m_+ = \frac{u_{i+1} - u_i}{\Delta x}, \tag{27}$$

where u is one of the state variables in the vector $\mathbf{u}$; note that each quantity is interpolated independently. If these slopes have different signs, cell i is a local extremum, and we set $m_i = 0$. Otherwise, we calculate the harmonic mean of the neighboring slopes,

$$m_i = \frac{2m_+m_-}{m_+ + m_-}. \tag{28}$$

Van Leer also suggested a clever way of rewriting the harmonic mean to efficiently incorporate the logic deciding if the slopes have the same sign into the formula:

$$m_i = \frac{|m_-|m_+ + m_-|m_+|}{|m_+| + |m_-|}. \tag{29}$$

On some computer systems, Eq. (29) is much faster than Eq. (28). The slopes m_i are then used to calculate a new vector $\mathbf{u}$ at the cell interfaces for use in Eq. (24) (or Eq. (25)). Each term in $\mathbf{u}$ is calculated as

$$u_{i\pm1/2} = u_i \pm \frac{\Delta x}{2} m_i, \tag{30}$$

depending on whether $\mathbf{u}$ is needed at the left or right cell interface. Thus, at interface $i + 1/2$ Eq. (30) gives us $\mathbf{u}_\ell = \mathbf{u}_i + \mathbf{m}_i\Delta x/2$ and $\mathbf{u}_r = \mathbf{u}_{i+1} - \mathbf{m}_{i+1}\Delta x/2$, where $\mathbf{m}_i$ is a vector of slopes with Eq. (29) for each moment.

3.2. A simple multidimensional Riemann solver

Now the fluxes $\mathbf{A}_x\mathbf{u}_{i\pm1/2,j}$ and $\mathbf{A}_z u_{i,j\pm1/2}$ can each be computed using the flux derived from the one-dimensional analysis resulting in Eq. (25), and the eigenstructure used in the correction term is evaluated using the one-dimensional problem implied by each term in Eq. (18). The fluxes are

$$\mathbf{A}_x\mathbf{u}_{i+1/2,j} = \mathbf{A}_x \frac{\mathbf{u}_{i,j} + \mathbf{u}_{i+1,j}}{2} - \frac{1}{2}\left[\sum_k \mathbf{r}_{x,k}|\lambda_{x,k}|\mathbf{l}_{x,k}\right](\mathbf{u}_{i+1,j} - \mathbf{u}_{i,j}) \tag{31}$$

and

$$\mathbf{A}_z\mathbf{u}_{i,j+1/2} = \mathbf{A}_z \frac{\mathbf{u}_{i,j} + \mathbf{u}_{i,j+1}}{2} - \frac{1}{2}\left[\sum_k \mathbf{r}_{z,k}|\lambda_{z,k}|\mathbf{l}_{z,k}\right](\mathbf{u}_{i,j+1} - \mathbf{u}_{i,j}). \tag{32}$$

The interpolation for the higher order method is only done in the direction normal to the cell face; any conservative interpolation scheme will preserve the face average in the tangent direction. This method can also be extended to non-uniform grids, but this is not done here for simplicity.

Because the P_N equations are linear, the Roe matrix (and its eigenstructure) is constant. Much of Eqs. (31) and (32) can therefore be precomputed. Again, some insight may be gained by looking at the specific example of P_1. Using Eq. (16) allows us to build the matrix used in the correction term in Eq. (32) for the Jacobian $\mathbf{A}_z$,

$$\sum_k \mathbf{r}_{z,k}|\lambda_{z,k}|\mathbf{l}_{z,k} = \begin{bmatrix} \frac{1}{\sqrt{3}} & 0 & 0 \\ 0 & \frac{1}{\sqrt{3}} & 0 \\ 0 & 0 & 0 \end{bmatrix}. \tag{33}$$

In this case the correction adds some dissipation equal to the difference between the two neighboring cell states times the absolute value of the eigenvalue. Because there is no x momentum transported in the z direction, the is no dissipation for that term.

The time integration is handled explicitly, and a second-order Runge–Kutta method [15] was used to allow larger time steps than are allowed by a simple forward Euler scheme. The source term, $\mathbf{S}_{i,j}(\mathbf{u}_{i,j})$ in Eq. (18), is evaluated at the beginning of the time step using the cell-centered $\mathbf{u}_{i,j}$, so for the radiation transport equation

$$\mathbf{S}_{i,j} = \begin{bmatrix} (\Sigma_s - \Sigma_t)\psi_0^0(x_{i,j}) \\ -\Sigma_t\psi_1^0(x_{i,j}) \\ \cdots \\ -\Sigma_t\psi_l^m(x_{i,j}) \\ \cdots \\ -\Sigma_t\psi_N^m(x_{i,j}) \end{bmatrix}. \tag{34}$$

3.3. Extra dissipation

Riemann solvers sometimes have problems with waves that have zero speed. The reason why is evident in Eq. (33); there are some terms that do not have any dissipation. The lack of dissipation can cause some unphysical solutions to develop. There are several fixes to this problem in the Riemann solver community, but they tend to be either problem-specific, like Powell's $\nabla \cdot \mathbf{B} = 0$ fix for the multidimensional magnetohydrodynamics equations [16], or they apply to nonlinear systems where an eigenvalue passes through zero, like the entropy fix [13,1]. Because our system is linear, a specific fix is proposed: If we replace the zero eigenvalue in Eq. (33) with $1/\sqrt{3}$, we get

$$\sum_k \mathbf{r}_k|\lambda_k|\mathbf{l}_k = \begin{bmatrix} \frac{1}{\sqrt{3}} & 0 & 0 \\ 0 & \frac{1}{\sqrt{3}} & 0 \\ 0 & 0 & \frac{1}{\sqrt{3}} \end{bmatrix}. \tag{35}$$

This essentially changes the method from a purely Roe-type Riemann solver to one where the terms with non-zero eigenvalues are treated with a Roe-type solver and the ones with zero eigenvalues are updated using a Lax–Friedrichs solver [1,17]. This change does not increase the order of the error of the method; we are only adding on another error of the same size that acts like a diffusive term. It is important to note that this fix is only used to eliminate some unphysical aspects of the numerical solutions; even the solutions obtained without this fix are excellent.

We can extend this idea to higher order P_N approximations, where the zero eigenvalues are replaced with the smallest non-zero eigenvalue.

4. Results

The first problem is the simplest: a pulsed line source. This simple problem highlights the key features of the Riemann solver and shows some interesting characteristics of the spherical harmonics approximation.

This problem clearly shows the importance of the high-resolution scheme. The second problem is loosely based on a lattice core. This problem shows that there are significant deficiencies in using just the P_1 approximation.

4.1. The line source in two dimensions

The most basic of all time dependent problems is a Green's function problem, in which a pulse of particles is emitted from a line in an infinite medium. In a linear system, solutions to all other time dependent problems are just superpositions of such Green's functions. Only purely scattering material is considered here; in an infinite homogeneous medium absorption can be scaled out by setting $\psi = \psi' e^{-\Sigma_a t}$, where ψ' is the pure scattering solution.

The scalar flux can be solved for analytically in a few special cases. In a vacuum, where $\Sigma_t = 0$, the P_1 equations, written in cylindrical coordinates, can be reduced to a wave equation, namely

$$\frac{\partial^2 \phi}{\partial^2 t} + \frac{1}{3r}\frac{\partial}{\partial r} r \frac{\partial \phi}{\partial r} = 0. \tag{36}$$

This can be solved using a Hankel transform [18] yielding

$$\phi(r,t) = \frac{3\phi_0}{2\pi}\left(\frac{\delta(t-\sqrt{3}r)}{\sqrt{t^2-3r^2}} - t\frac{h(t-\sqrt{3}r)}{(t^2-3r^2)^{3/2}}\right), \tag{37}$$

where h is the unit step function. This is a very surprising result; the scalar flux is composed of two parts, the first is a delta function pulse of uncollided particles, but the other part is negative! No matter how strong the scattering term is, it is always possible to find a t small enough such that the scattering is negligible, and the scalar flux will then be negative. For short times, not many of the neutrons have undergone scattering yet. The distribution is not linearly anisotropic (all the neutrons are moving away from the line source and none toward it), and the P_1 equations are not a good approximation to the physical system under these conditions. This negative scalar flux is a manifestation of this breakdown of the P_1 equations. Similar expressions can also be found for higher orders of the spherical harmonic expansion.

To test the two-dimensional Riemann solver, this Greens function problem was solved using the second-order-in-space Riemann solver on a Cartesian x–z grid. The time step in the second-order Runge–Kutta time integration used here was chosen small enough such that the time discretization errors were extremely small. The exact solution is of course just a function of radius r, but this symmetry was not exploited, and the second-order scheme produced very good symmetry despite the Cartesian grid. For comparison, the transport theory scalar flux was computed using Ganapol's solution [19–21] and various orders of spherical harmonics. Because of the radial symmetry, only the solution along the x-axis is shown in the plots.

For the first problem $\Sigma_t = \Sigma_s = 0$, so that we can compare to Eq. (37). Fig. 1 shows the analytic and numerical solution to this problem. Even though the P_1 equations do not adequately model the physical system, we can see that the Riemann solver accurately estimates the analytic P_1 solution to this difficult problem. Riemann solvers were designed to handle shocks well; we see here that they also deal with the multiple singularities in Eq. (37) extraordinarily well. As the resolution of the spatial grid is refined, the solution even more closely approximates the analytic solution.

The scattering cross-section is set to $\Sigma_s = 1\ \mathrm{cm}^{-1}$ for the remainder of the line source problems. The scalar flux at 1 and 10 s after the pulse from the line source is shown in Figs. 2 and 3. Early on (at about one mean scattering time), none of the P_N results is a good approximation to the transport solution; they all contain significant negative components. As time progresses, however, after most of the neutrons have undergone several scattering collisions, the spherical harmonics equations give much better approximations to the true solution. It is quite remarkable that the Riemann solver calculated the solution accurately

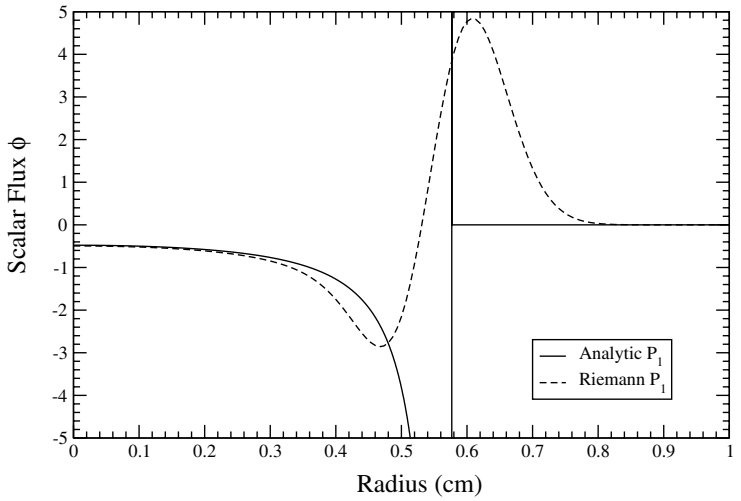

Fig. 1. The scalar flux from a line source in a vacuum calculated with P_1 analytically and numerically at one second after the pulse. The delta function is located at radius $r = 1/\sqrt{3}$. Note that the flux is negative in both the numerical and analytic solutions.

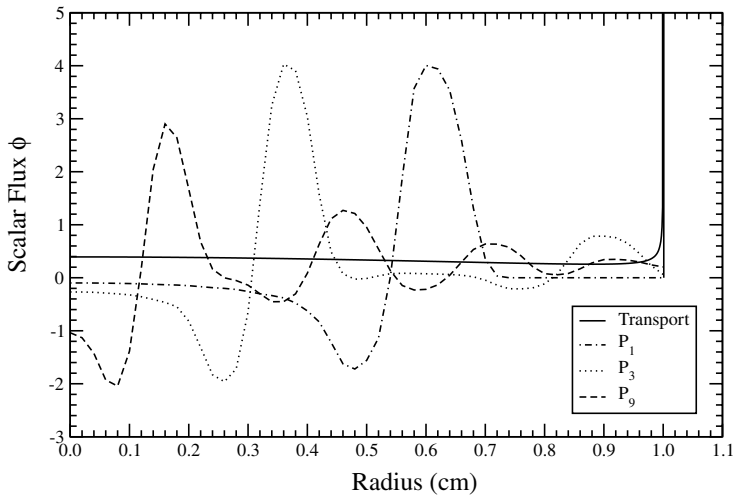

Fig. 2. The scalar flux from a line source with $\Sigma_s = 1\ \text{cm}^{-1}$ calculated numerically with P_1, P_3, and P_9 expansions one second after the pulse. These are compared to Ganapol's analytic solution. Note that the flux for the P_N closures is negative.

enough early (in the non-physical regime) to allow the solutions at later times to be very good. It should be noted that in the transport solution there is a shell of uncollided particles moving away from the line source with speed $v = 1$. The pulse of neutrons at the wave front, which can be seen in Fig. 2, represents a singularity in the analytic solution to the transport problem. This wave front dies away at later times.

In two dimensions the number of unknowns increases proportionally to Δx^{-2} as Δx is decreased, and the high-resolution scheme becomes absolutely vital in order to resolve features of the solutions without needing an extremely fine mesh. The high-resolution calculation shows the expected structure of pulses moving

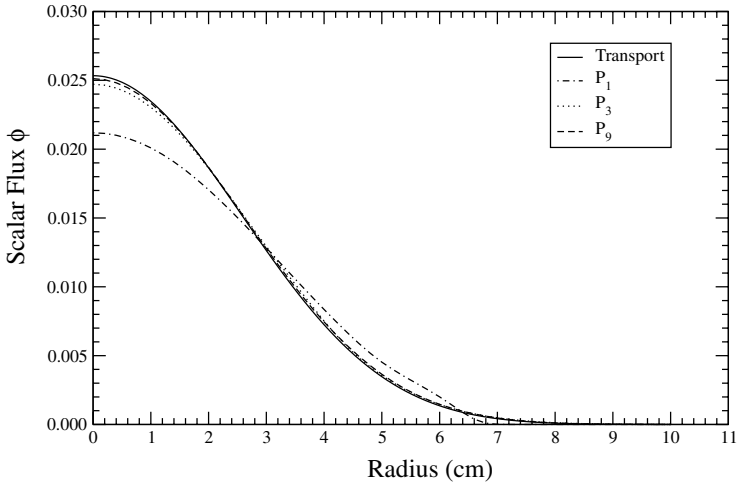

Fig. 3. The scalar flux from a line source with $\Sigma_s = 1\ \mathrm{cm}^{-1}$ calculated numerically with P_1, P_3, P_9 expansions 10 s after the pulse. These are compared to Ganapol's analytic solution.

away from the center, while the first-order calculation shows none of this. Fig. 4 shows the same pulsed line source calculation as above, with 50 cells per centimeter. The ring structure of the P_N solution is clear in the high-resolution solution and completely absent in the first-order solution. Even if the number of cells is doubled to 100 per centimeter, the first-order solution is not as good the high-resolution solution with 50 cells per centimeter.

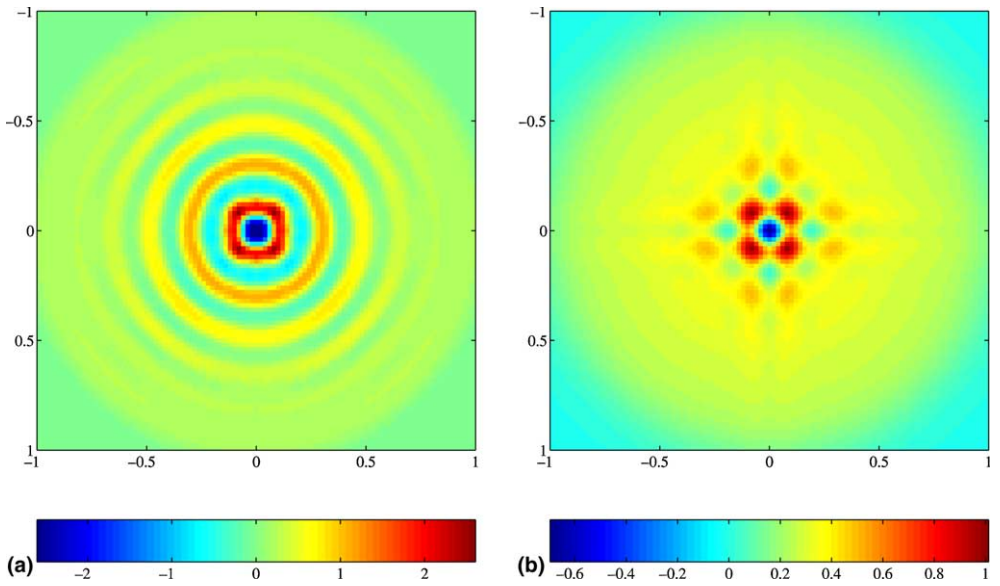

Fig. 4. The scalar flux from a line source with $\Sigma_s = 1\ \mathrm{cm}^{-1}$ from a P_{15} calculation. The ring structure of the P_N solution is clear in the high-resolution solution and completely absent in the first-order solution. (a) High res., 50 cells/cm, (b) low res., 50 cells/cm.

4.2. A lattice problem

This problem is a checkerboard of highly scattering and highly absorbing regions loosely based on a small part of a lattice core. The system is seven centimeters wide. The bulk of the lattice is composed of a scattering material with $\Sigma_t = \Sigma_s = 1\ \text{cm}^{-1}$. There are 11 absorbing regions where $\Sigma_t = \Sigma_a = 10\ \text{cm}^{-1}$. At time zero, a source of strength one is turned on in the central region of the system. All neutrons travel at $v = 1$ cm/s, and the problem is surrounded on all sides by vacuum boundaries.

Fig. 5 shows the scalar flux 3.2 s after the source is turned on. For comparison with the P_N calculations, this problem was also computed using two different methods. First, a diffusion calculation with a simplified Levermore–Pomraning flux limiter was done using the ALEGRA code [22] which used the same grid as the P_N calculations. Second, an implicit Monte Carlo calculation was done using the KULL IMC package [23]. The simulation consisted of 36 million particles in half the problem domain, with a reflective boundary on the center line.

The P_{15} calculation shows distinct shadows behind the absorbers in addition to well-defined beams of neutrons leaking between the corners of the absorbing regions; this agrees very well with the Monte Carlo

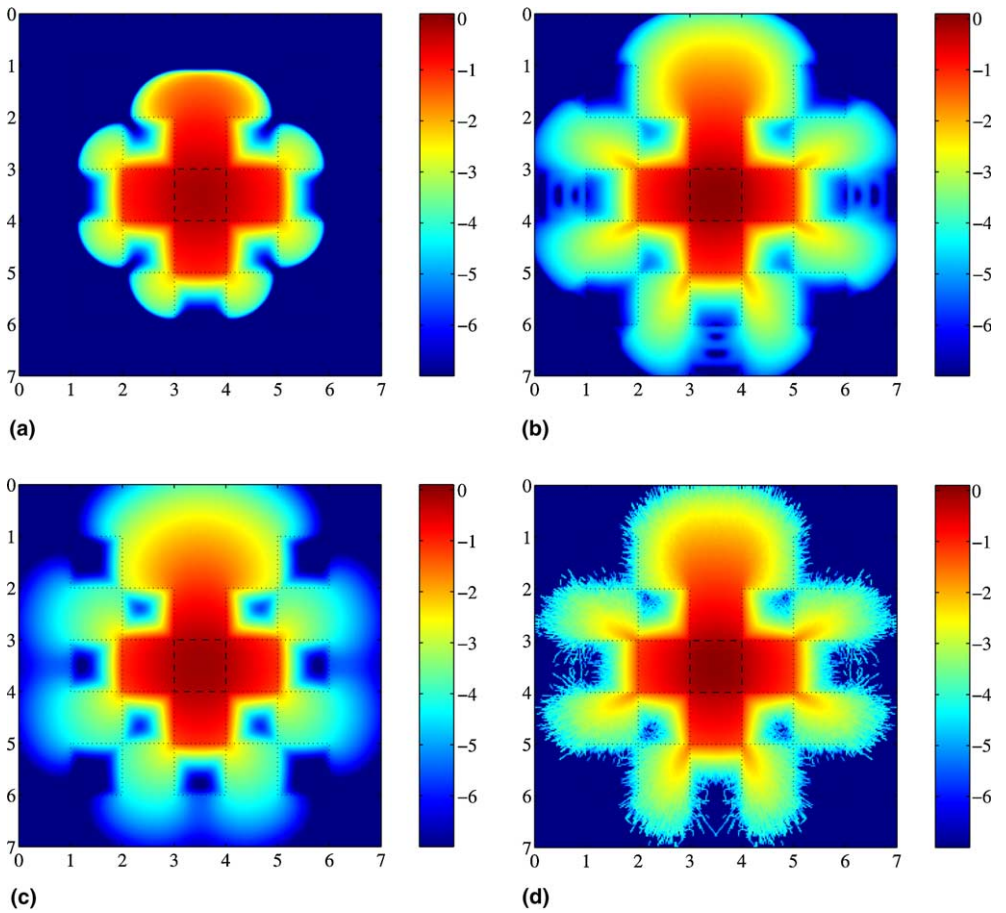

Fig. 5. The scalar flux calculated in the lattice problem 3.2 s after the source was turned on. The gray scale map is proportional to $\log_{10}\phi$ and limited to seven orders of magnitude. (a) P_1, (b) P_{15}, (c) flux limited diffusion, and (d) implicit Monte Carlo.

simulation, especially for scalar fluxes above 10^{-4} particles/cm^2 s. The P_1 calculation is much too diffuse throughout the simulation. The scalar flux computed using P_1 has an artificial wave front of neutrons traveling at speed $v = 1/\sqrt{3}$ cm/s. This is due to the fact that in P_1, the neutron waves travel only at this speed. In the P_{15} calculation, the neutron waves can travel at many more speeds, eliminating these non-physical wave fronts. The flux limited diffusion solution captures the wave front very well (Fig. 5(c)), but fails to capture the beams leaking between the absorbers that can be seen in the P_{15} and Monte Carlo calculations. In regions of low flux, Fig. 5(b) shows some oscillations in the flux on the order of $\phi = 10^{-6}$ particles/cm^2 s; these oscillations are related to the ones in the line source problem (Fig. 2).

5. Conclusions

We have developed a numerical method to solve the time dependent spherical harmonics equations in two-dimensions using a high-order Riemann solver. The method is based on exactly treating the streaming terms from the spherical harmonics equations in one-dimension, and using these results to compute the flux of state across computational cells. The use of a harmonic-mean slope-limiter allows the method to be second-order in space; a second-order explicit Runge–Kutta time integration is used. The method deals with even singular solutions quite robustly.

The method has been compared to exact Greens functions of the P_1 equations and benchmark transport theory solutions, as a function of spherical harmonics order. These results show that the time dependent spherical harmonics equations can be successfully solved with a Riemann solver, and illustrate the inadequacy of the lowest order P_N approximations for time dependent transport simulations: particles in the P_1 approximation move only at the speed $1/\sqrt{3}$, which is rather limited compared to the whole range $[0, 1]$ of physical possibility. This is of course a reflection of the limited angular resolution of P_1 theory – the two-dimensional P_{15} results contain eight separate speeds, reflecting their higher angular resolution. A comparison of the results of time dependent P_1 and P_{15} theory in the alternating scatterers and absorbers of Fig. 5 shows the improved spatial resolution of the scalar flux that comes from having greater angular resolution.

References

[1] R.J. LeVeque, Numerical Methods for Conservation Laws, Birkhäuser Verlag, 1992.
[2] I. Toumi, A. Bergeron, D. Gallo, E. Royer, D. Caruge, FLICA-4: a three-dimensional two-phase flow computer code with advanced numerical methods for nuclear applications, Nuclear Engineering and Design 200 (2000) 139–155.
[3] D.S. Balsara, An analysis of the hyperbolic nature of the equations of radiation hydrodynamics, Journal of Quantitative Spectroscopy and Radiative Transfer 61 (5) (1999) 617–627.
[4] D.S. Balsara, Linearized formulation of the Riemann problem for radiation hydrodynamics, Journal of Quantitative Spectroscopy and Radiative Transfer 61 (5) (1999) 629–635.
[5] W.W.L. Dai, P.R. Woodward, Numerical simulations for radiation hydrodynamics – II. Transport limit, Journal of Computational Physics 157 (1) (2000) 199–233.
[6] T.A. Brunner, J.P. Holloway, One-dimensional Riemann solvers and the maximum entropy closure, Journal of Quantitative Spectroscopy and Radiative Transfer 69 (2001) 543–566.
[7] T.A. Brunner, J.P. Holloway, Two new boundary conditions for use with the maximum entropy closure and an approximate Riemann solver, PHYSOR 2000, ANS International Topical Meeting on the Advances in Reactor Physics and Mathematics and Computation into the Next Millennium, American Nuclear Society, 2000.
[8] K.O. Ott, Introductory Nuclear Reactor Statics, revised ed., American Nuclear Society, 1989.
[9] E.E. Lewis, W.F. Miller Jr., Computational Methods of Neutron Transport, Wiley, New York, 1994.
[10] G.I. Bell, S. Glasstone, Nuclear Reactor Theory, Krieger, 1970.
[11] T.A. Brunner, Riemann solvers for time-dependent transport based on the maximum entropy and spherical harmonics closures, Ph.D. Thesis, University of Michigan, 2000.

[12] P. Roe, A brief introduction to high-resolution schemes, in: M.Y. Hussaini, B. van Leer, J. Van Rosendale (Eds.), Upwind and High-resolution Schemes, Springer, Berlin, 1997.
[13] B. van Leer, W.-T. Lee, K.G. Powell, Sonic-point capturing, in: AIAA 9th Computational Fluid Dynamics Conference, 1989.
[14] B. van Leer, Towards the ultimate conservative difference scheme. V. A second-order sequel to Godunov's method, Journal of Computational Physics 32 (1979) 101–136.
[15] C. Canuto, M.Y. Hussaini, A. Quarteroni, T.A. Zang, Spectral Methods in Fluid Dynamics, Springer, Berlin, 1988.
[16] K.G. Powell, An approximate Riemann solver for magnetohydrodynamics (that works in more than one dimension), in: M.Y. Hussaini, B. van Leer, J. Van Rosendale (Eds.), Upwind and High-resolution Schemes, Springer, Berlin, 1997.
[17] K. Murawski, T. Tanaka, Modern numerical schemes for solving magnetohydrodynamic equations, Astrophysics and Space Science 254 (1997) 187–210.
[18] L. Debnath, Integral Transforms and Their Applications, CRC Press, Boca Raton, FL, 1995.
[19] B.D. Ganapol, Solution of the one-group time-dependent neutron transport equation in and infinite medium by polynomial reconstruction, Nuclear Science and Engineering 92 (1986) 272–279.
[20] B.D. Ganapol, K.L. Peddicord, The generation of time-dependent neutron transport solutions in infinite media, Nuclear Science and Engineering 64 (1977) 317–331.
[21] B.D. Ganapol, Homogeneous infinite media time-dependent analytic benchmarks for X-TM transport methods development, Los Alamos National Laboratory, March, 1999.
[22] T.A. Brunner, T.A. Mehlhorn, A user's guide to radiation transport in ALEGRA-HEDP, version 4.6, Technical Report SAND-2004-5799, Sandia National Laboratories, Albuquerque, NM, November, 2004.
[23] N.A. Gentile, N. Keen, J. Rathkopf, The KULL IMC package, Technical Report UCRL-JC-132743, Lawrence Livermore National Laboratory, Livermore, CA, 1998.